AGU100 ADVANCING EARTH AND SPACE SCIENCE

Space Weather

RESEARCH ARTICLE
10.1029/2018SW001814

Transformer-Level Modeling of Geomagnetically Induced Currents in New Zealand's South Island

T. Divett[1], G. S. Richardson[2], C. D. Beggan[2], C. J. Rodger[1], D. H. Boteler[3], M. Ingham[4], D. H. Mac Manus[1], A. W. P. Thomson[2], and M. Dalzell[5]

[1]Department of Physics, University of Otago, Dunedin, New Zealand, [2]British Geological Survey, Edinburgh, UK, [3]Geomagnetic Laboratory, Natural Resources Canada, Ottawa, Canada, [4]School of Chemical and Physical Sciences, Victoria University of Wellington, Wellington, New Zealand, [5]Transpower New Zealand Ltd., Wellington, New Zealand

Abstract During space weather events, geomagnetically induced currents (GICs) can be induced in high-voltage transmission networks, damaging individual transformers within substations. A common approach to modeling a transmission network has been to assume that every substation can be represented by a single resistance to Earth. We have extended that model by building a transformer-level network representation of New Zealand's South Island transmission network. We represent every transformer winding at each earthed substation in the network by its known direct current resistance. Using this network representation significantly changes the GIC hazard assessment, compared to assessments based on the earlier assumption. Further, we have calculated the GIC flowing through a single phase of every individual transformer winding in the network. These transformer-level GIC calculations show variation in GICs between transformers within a substation due to transformer characteristics and connections. The transformer-level GIC calculations alter the hazard assessment by up to an order of magnitude in some places. In most cases the calculated GIC variations match measured variations in GIC flowing through the same transformers. This comparison with an extensive set of observations demonstrates the importance of transformer-level GIC calculations in models used for hazard assessment.

Key Points:
- We develop a transformer-level network representation of New Zealand's South Island electrical transmission network to examine GIC
- Modeling GIC at the transformer-level can significantly alter the perception of the GIC hazard compared to simpler substation-level modeling
- We found reasonable agreement between extensive measurements of GIC and modeled transformer-level GIC across multiple storms

Correspondence to:
T. Divett,
tim.divett@otago.ac.nz

Citation:
Divett, T., Richardson, G. S., Beggan, C. D., Rodger, C. J., Boteler, D. H., Ingham, M., et al. (2018). Transformer-level modeling of geomagnetically induced currents in New Zealand's South Island. *Space Weather*, *16*, 718–735. https://doi.org/10.1029/2018SW001814

Received 25 JAN 2018
Accepted 12 MAY 2018
Accepted article online 20 MAY 2018
Published online 20 JUN 2018

1. Introduction

During space weather events the interaction of coronal mass ejections and high-speed streams with the Earth's magnetic field gives rise to electric currents flowing in the ionosphere and magnetosphere. The magnetic field variations associated with these currents during geomagnetic disturbances induce an electric field at the Earth's surface through an interaction with the conducting ground. The electric field induced during these disturbances leads to an electromotive force in long conductors such as electrical transmission lines causing currents to flow along the conductors. These geomagnetically induced currents (GICs) can cause a direct current (DC) offset current to flow through the windings of transformers connected to the transmission lines at substations. GIC can damage transformers through magnetic saturation of the material in the transformer's core, which leads to overheating and generation of harmonics. GICs have been observed at low to middle geomagnetic latitude countries including the United Kingdom (Erinmez et al., 2002), South Africa (Koen & Gaunt, 2003), Brazil (Trivedi et al., 2007), China (Liu et al., 2009), Spain (Torta et al., 2012), and Australia (Marshall et al., 2013), as well as New Zealand (Beland & Small, 2004; Manus Mac et al., 2017; Marshall et al., 2012). In New Zealand, during the November 2001 storm a single phase of Halfway Bush's (HWB's) transformer T4 was damaged, subsequently written off and replaced.

Modeling GIC is useful to understand the impact of geomagnetic storms on power systems. A standard approach to modeling GIC, used, for example, by Koen and Gaunt (2003), Torta et al. (2012), Beggan et al. (2013), Blake et al. (2016), Bailey et al. (2017), and Divett et al. (2017), has been to use the method of Lehtinen and Pirjola (1985; LP85 hereafter). In these applications of the LP85 method substations are approximated as a single resistance to Earth and it is usually assumed that equal levels of GIC flow through each transformer in a substation. This approach was used to model the GICs due to a uniform magnetic field variation for the South Island in Divett et al. (2017). In that study the substation-level GICs at each earthed substation were calculated for a range of directions of the magnetic field.

Transpower New Zealand Ltd have measured GICs through multiple individual transformers within substations (Manus Mac et al., 2017; Rodger et al., 2017). It is important to note that these GIC observations are of the GIC flowing through individual transformers (transformer-level GIC) rather than a total measure of GIC to ground for each substation (substation-level GIC). This is an important consideration when comparing modeled GIC to observed GIC. Manus Mac et al. (2017) showed that the GICs through different transformers can be substantially different, even within the same substation at the same moment in time.

It is therefore important to model GIC at the transformer level rather than the substation level for four reasons:

1. Individual transformers are impacted differently during storms.
2. Power transformers are generally all different (e.g., age, resistances, winding type, and power characteristics).
3. Observations of GIC are usually conducted at individual transformers.
4. With this level of modeling, we will eventually be able to predict which transformers will be worst affected by geomagnetic disturbances during a large storm.

Boteler and Pirjola (2014) showed how autotransformers and normal transformers connected within a hypothetical substation can be represented in an adaptation of the LP85 method. Boteler and Pirjola (2017) (hereafter BP17) went on to show how to calculate the transformer-level GIC. BP17 then showed how this method could be used to demonstrate the influence of the geomagnetic coast effect on power networks using a hypothetical square network as well as for the test case network of Horton et al. (2012). More recently, Richardson and Beggan (2017) confirmed that the LP85 method used to model GIC in the United Kingdom, Ireland, Austria, and New Zealand (Bailey et al., 2017; Beggan et al., 2013; Blake et al., 2016; Divett et al., 2017) correctly calculates the transformer-level current of the test case in Horton et al. (2012). It is this implementation of LP85, which we extend in the present study. We shall demonstrate the use of transformer-level GIC calculations within a model of an existing network. The South Island is ideal for this demonstration because it is small and isolated.

Commercial power engineering packages have been used to model transformer-level GIC in real networks in the past. For instance Overbye et al. (2012) used the PowerWorld package to model the transformer-level GIC flowing in the North American Eastern Interconnect due to a uniform electric field across the region. Overbye et al. (2012) point out that the modeling of GIC will be greatly enhanced by comparison with observations. Butala et al. (2017) provided comparison of observed and modeled transformer-level GIC using PowerWorld in the same network, also with a uniform electric field. In a further example, Shetye and Overbye (2015) modeled GIC in the same network using a single resistance for each substation. They applied the nonuniform, North American Electric Reliability Corporation (NERC) geomagnetic disturbance benchmark electric field across the region but did not compare their GIC calculations with measured GIC. In the present study we compare modeled GIC with Transpower's observations across multiple geomagnetic storms showing detail of GICs in each transformer at case study substations. This has been uniquely possible due to Transpower allowing publication of not only the GIC observations but also details of the network configuration. We believe the present study is the first to compare an aggregate of GIC observations across multiple storms with transformer-level GIC modeling using a nonuniform electric field incorporating variation due to ground conductance. Further, the present study demonstrates a path for researchers who currently use the LP85 method to calculate transformer-level GIC—including the geophysical step of calculating the geoelectric field. Hence, we provide a different implementation of the calculations that are common in commercial packages that currently do not include the geophysical step.

The electric field that we use in the present paper to drive the network model was calculated by Divett et al. (2017) using the thin-sheet modeling approach of Vasseur and Weidelt (1977). This approach had also been used successfully to calculate geoelectric fields for GIC in the United Kingdom, and in Austria by Beggan et al. (2013), Mckay (2003), and Bailey et al. (2017), respectively. Divett et al. (2017) compared the output of the thin-sheet model to field studies by comparing against induction vectors measured by Chamalaun and McKnight (1993), finding good agreement in magnitude and direction. However, Divett et al. (2017) did note some errors in the direction of calculated fields at the coast compared to measured induction vectors, which was inferred to be due to the relative coarseness of the modeled coastline in the thin-sheet conductance model. The strongest electric fields were found to occur when the driving geomagnetic field variation was aligned parallel to the main axis of New Zealand. This direction is only 25° to 30° east of present-day geomagnetic north in the New Zealand region and hence is close to the geomagnetic north magnetic field direction

expected to be induced by an east-west auroral electrojet. The electric field in this case is roughly perpendicular to the west and east coasts, therefore resulting in the greatest amplification of the electric field by the coast effect.

In the present study we have developed a transformer-level representation of the high-voltage electrical transmission network of New Zealand's South Island. We calculate both substation-level and transformer-level GIC using the transformer-level network representation. We compare the GICs calculated from the original substation-level network representation with the transformer-level network and the ratios of observed GICs in transformers at Islington (ISL) and HWB substations reported by Manus Mac et al. (2017) and Rodger et al. (2017). We demonstrate the importance of this transformer-level modeling to GIC calculations through this comparison. By presenting the transformer-level GIC details of three substations we show why GICs vary between different transformers within a substation. We believe the present study is the first to compare extensive observations with transformer-level GIC modeling using a nonuniform electric field incorporating variation due to ground conductance.

2. GIC Observations at the Transformer Level

The New Zealand GIC data are particularly extensive in an international context. These observations are nearly continuous since 2001 at up to 58 individual transformers. The measurements were initially intended to monitor currents in the Earth return path of the high-voltage DC link between the North and South Islands. By removing the impact of the high-voltage DC (HVDC) earth return currents from the data the remaining current is GIC (Manus Mac et al., 2017).

In the introduction we suggest why it is important to model GIC at the transformer level rather than the substation level. One of the points we note is that the GICs observed in the same substation are different for each transformer in that substation. This is commonly seen in the New Zealand data. It is possible to see this variation due to the large number of transformers that are monitored within substations in New Zealand. The variation is caused by the difference in the resistances of each transformer and its connection to Earth. Evidence of these differences has been previously presented in the literature. For example, Manus Mac et al. (2017) examined how stray HVDC currents entered into South Island transformers. Figure 4 of their paper shows the stray HVDC current seen at each transformer for a fixed level of HVDC earth return current. The figure demonstrates that is possible to have different levels of current in each of the instrumented transformers within the same substation. Varying GIC current magnitudes inside a single substation are also presented in their paper for two example storms: 6 November 2001 (Figure 5 of Manus Mac et al., 2017) and 2 October 2013 (Figure 7 of Manus Mac et al., 2017).

To provide further evidence, we examine observations of peak GIC at the ISL substation, as shown in Table 1. This table shows the magnitude of peak GIC through each of the four instrumented transformers at ISL for five recent storms. These measurements demonstrate that there is a significant variation in the GIC magnitude in individual transformers within the same substation during geomagnetic storms. These observations of the GICs have been corrected for HVDC earth return current (Manus Mac et al., 2017). Measurements of GICs through T6H and T7H were not available from 7 September 2017 as a fault occurred in the logging and archiving equipment.

Trends in the relative magnitude and ratio of GIC through each transformer are clear across all five storms in Table 1. T3H and T7H experience similar levels of GIC. However, the GIC through T6H is 3 times that through T3H. On the other hand, GIC through T9H is one third that through T3H in all but the 2 October 2013 storm. Therefore, there is a factor of approximately 9 between the peak GIC at T6H to T9H, which is a significant difference in the amplitude of GIC. These values suggest that there are consistent ratios between the GICs observed at each transformer in the same substation for multiple storms. We note that the values are not identical from storm to storm and suggest that this may be due to differences in the geomagnetic forcing from storm to storm. One example of these differences between storms is the distributions of magnetic frequency components present, which are expected to couple to each transformer differently due to transformer frequency response factors. Previously, it was reported by Rodger et al. (2017) that the peak GIC measured at HWBT4L was consistently 3 times larger than ISLT6H. These ratios of GICs through different transformers during several storms provide a useful measure to compare against modeled GICs due to the consistent trend over several storms.

Table 1
Peak GIC (in Amperes) Through Transformers at Islington (ISL) During Five Recent Large Storms (Times Given in UT)

Time, UT	T3H	T6H	T7H	T9H
2 October 2013 1:56	5.5	19.1	—	4.0
17 March 2015 4:46	6.4	17.0	5.7	2.2
22 June 2015 18:34	4.4	12.2	3.7	1.4
7 September 2017 23:02	6.6	—	—	2.4
8 September 2017 12:41	6.6	—	—	0.5

Note. Dashes indicate no data were available. The H in the transformer name indicates the high-voltage winding.

3. Method: Developing a Transformer-Level GIC Network Representation of the South Island From a Substation-Level Representation

We have developed a transformer-level network representation of the South Island's power transmission network. This is based on the substation-level nodal network approach of LP85 so that we can make use of their matrix calculation techniques. This substation-level representation was used to calculate GICs across the South Island of New Zealand by Divett et al. (2017). In our first modification to the LP85 method we make a transformer-level network representation of the South Island's electrical transmission network. In this representation a single phase of the high-voltage (220, 110, and 66 kV) windings of every transformer in the transmission network is accounted for. This technique is based on the Boteler and Pirjola (2014) technique for describing autotransformers and normal transformers in the node and connector model developed by LP85. In the second modification to the LP85 approach we use this transformer-level network representation to calculate the current through each individual transformer winding in the South Island using BP17's technique.

This approach was suitable in our case as we started with an existing implementation of LP85's matrix calculations for the South Island. Because of this making the modifications was a minor change. Boteler (2014) showed that GIC modeling can also be performed using the nodal admittance matrix method (e.g., Guile & Paterson, 1977) that is common in power industry packages. Boteler and Pirjola (2014) show that the LP85 method is mathematically equivalent to the nodal admittance matrix method and points out that the second method is often preferred by electrical engineers. Boteler and Pirjola (2014) also point out that the nodal admittance matrix method provides a clearer sequence of calculations to calculate the same transformer-level GIC, compared to the LP85 method.

The transformer-level GIC is the current that flows through a specific winding of a specific transformer within a given substation. On the other hand the substation-level GIC is the total GIC flowing to Earth through the Earth grid resistance (EGR), also called substation grounding resistance or earth ground resistance.

We have focused on key locations that Manus Mac et al. (2017) and Rodger et al. (2017) report as having high levels of observed GICs and have experienced documented disruption during geomagnetic storms in the past (Marshall et al., 2012). Transformer number 6 at ISL (ISLT6) shows relatively high observed GICs during geomagnetic storms. (Note, ISLT6 is called M6 in Manus Mac et al. (2017) and Rodger et al. (2017) based on an old Transpower naming convention, but we are calling it T6 for consistency with other transformer names.) Archived observations started at ISLT6 in November 2001, and thus, ISLT6 is one of the longest monitored transformers in the South Island network. The highest observed GIC through this transformer was during the 6 November 2001 storm, which was 33 A. Transformer number 4 at HWB (HWBT4) is the transformer that was written off, and subsequently replaced, after the 6 November 2001 storm (Beland & Small, 2004). Transpower have been measuring GICs at HWBT4 since 2013 (Manus Mac et al., 2017).

Figure 1 shows the location of all 64 substations in the South Island, marked by crosses. The 29 earthed substations are labeled, substations where the high-voltage transformers (>33 kV) are unearthed are not labeled. Transmission lines are assumed to follow a straight line between nodes, which is a commonly applied modeling approximation. The resistance of a single phase of each of the three-phase transmission line varies from 0.039Ω for the 220 kV line between OHB and the nearest unearthed substation to 7.1Ω for the 66 kV line connecting COL to the unearthed substation directly north of COL, shown in Figure 1 by varying colors. These locations and resistances are the same as those used in the substation-level GIC modeling of Divett et al. (2017).

Note that we discuss transformer windings in several places in this paper in reference to the high- or low-voltage winding of a transformer. In this context we are referring to the total turns of a transformer coil, rather than each individual winding (or turn) of a coil. In a two-winding transformer with high-voltage windings and core separate from the low-voltage windings and core (referred to here as normal transformers) the high side winding refers to the windings on the high-voltage side, while the low side winding refers to the windings on the low-voltage side. In autotransformers the winding between the 220- and 110 kV buses is called the series winding, while the winding between 110- and 0 kV buses is the common winding. We also refer to a bus

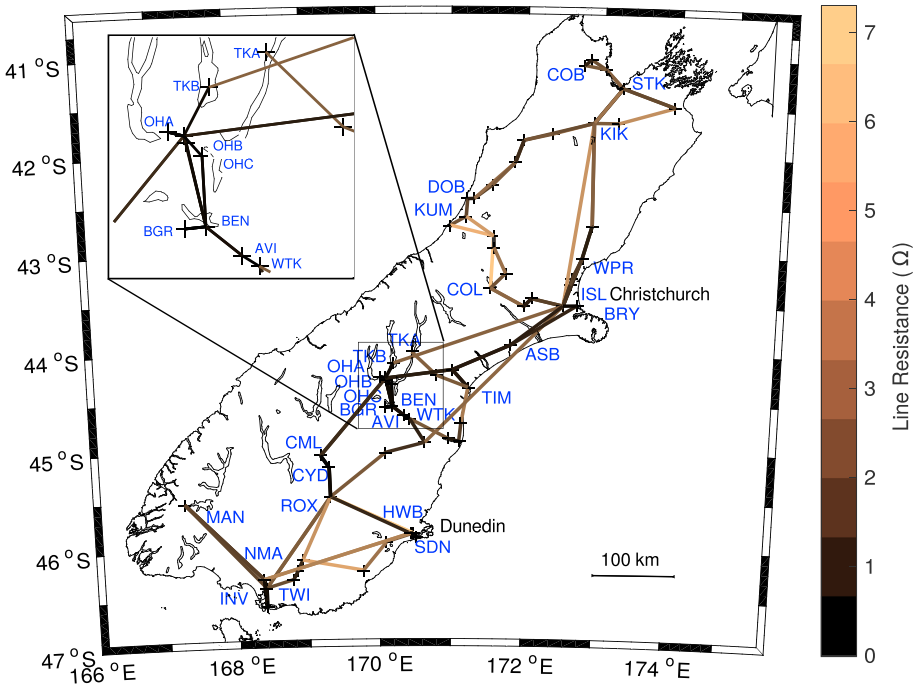

Figure 1. The South Island of New Zealand showing locations discussed in the text, transmission line resistance, and substation node locations (both provided by Transpower) in the South Island network representation. All 220-, 110-, and 66 kV lines are shown, although duplicate parallel lines are not. Unearthed substation locations are indicated with a cross without a label.

or busbar, meaning the three solid conductors, one for each phase, for distributing the currents between all the lines and all the transformer terminals within a substation. Finally, we also refer to a tap or center tap, meaning a contact made to a point part way along the windings of an autotransformer.

3.1. Modeled Geoelectric Fields for GIC Calculation

We drive the network representation by the electric fields calculated by Divett et al. (2017) in a domain around New Zealand discretized into 96 × 96 square grid cells. Cells are one sixth of a degree (roughly 20 km) in the north and east directions. This calculation used the thin-sheet model of Vasseur and Weidelt (1977), with a two-dimensional thin-sheet conductance model and depth variation specific to New Zealand's geology, based on magnetotelluric measurements, geology, and bathymetry. A uniform geomagnetic field variation was assumed. This driving magnetic field variation is uniform across the grid, with a period of 10 min and magnitude of 500 nT. We chose this period and amplitude to represent a moderately large geomagnetic disturbance. The direction of this geomagnetic field is 50° east of north, roughly parallel with the main axis of the South Island. The electric field variation calculated by this method is predominantly oriented to the northwest, roughly perpendicular to the South Island's main axis. This direction was chosen for this study because it gives the strongest electric field. Geomagnetic north varies from 21.5° to 25.5° east of geographic north from the south to the north of the South Island; hence, the direction of the driving magnetic field is 28.5° to 24.5° east of geomagnetic north respectively. The direction of the driving magnetic field will influence the relative intensity of GICs at each substation, as shown for New Zealand by Divett et al. (2017), and possibly for each transformer within a substation. For demonstration of the transformer-level GIC calculations we have chosen a single direction that is representative of a geomagnetic disturbance that would be expected to lead to large GICs.

The magnitude of Divett et al.'s (2017) calculated electric field varies around the South Island. The strongest electric field of ˜1.5 V/km occurs in the mountains of the Southern Alps to the west of Christchurch. These locations are shown on the map of the South Island in Figure 1. Near the coast there is localized deflection away from the northwest direction at locations where the coast is not oriented to the northeast, due to the coast effect (Mckay & Whaler, 2006; Parkinson & Jones, 1979).

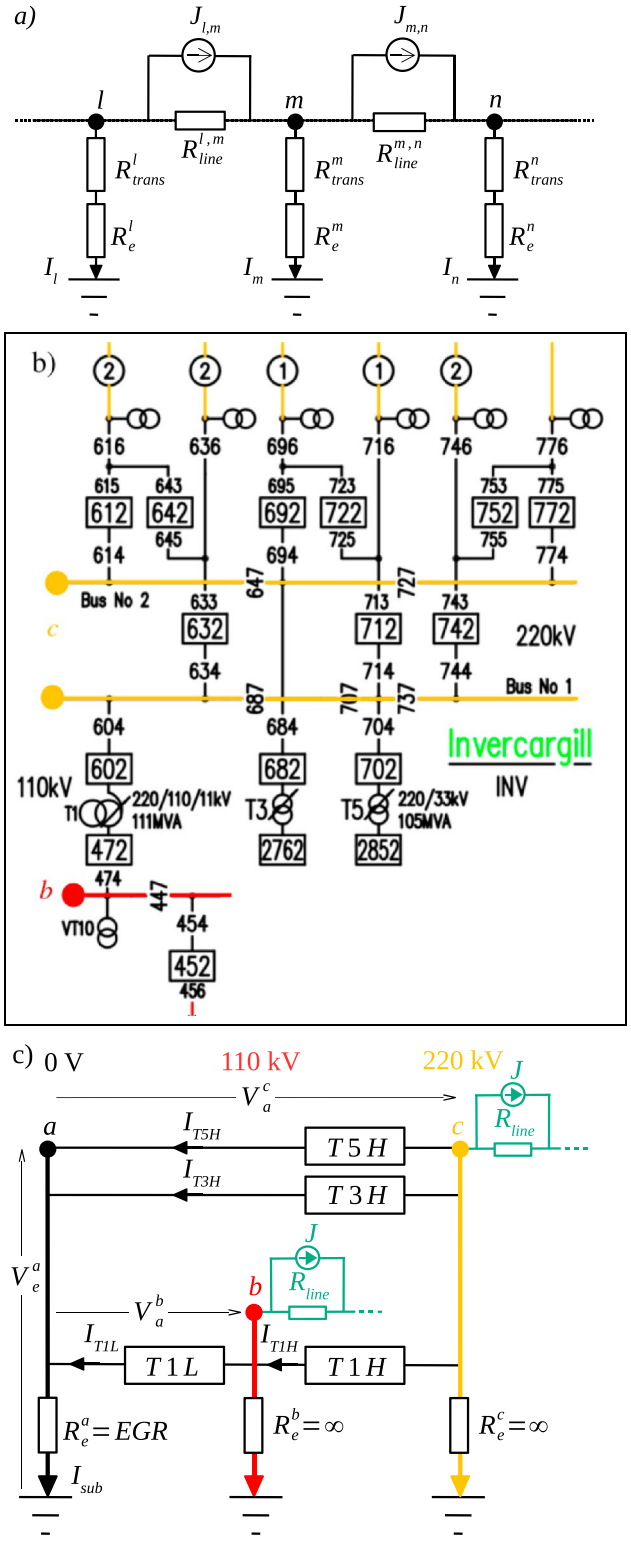

Figure 2. (a) The LP85 node and connector network representation, (b) the Single Line Diagram for an example substation (Invercargill, INV) extracted from a regional single line diagram where red lines are 110 kV and yellow lines are 220 kV, and (c) a block diagram showing how the direct current resistances of transformer windings at Invercargill can be represented as nodes connected by resistors to represent an autotransformer (T1's series winding [T1H] and common winding [T1L]) and the high-voltage side of parallel normal transformers T3 (T3H) and T5 (T5H) with multiple voltage nodes (0, 110, and 220 kV) within a substation. The green line resistors are representative of the multiple connections of the two high-voltage nodes to the rest of the network.

Table 2
Symbols Used in Our Study, Vectors Made of These Quantities Are Indicated by Overbars, Matrices in Bold

Symbol	Description
I_{sub}	Total GIC flowing to Earth at a substation, through the Earth grid resistance
I_{trans}	GIC flowing through a general transformer
I_{T1L}	GIC flowing through a specific transformer winding, in this case T1L
I_m^n	GIC flowing from node n to node m
$J_{m,n}$	Current source across the impedance of the transmission line connecting node m to n
V_m^n	Voltage difference between nodes n and m
V_e^a	Voltage at node a relative to local Earth for that substation
R_{trans}	Resistance of a general transformer winding
R_{sub}^n	Resistance of the nth substation (in LP85 substation-level calculations)
R_e^n	Resistance of the nth Earth grid resistance (in the transformer-level calculations)
R_{T1L}	Resistance of a specific transformer winding, in this case T1L
$R_{line}^{m,n}$	Resistance of the transmission line connecting nodes m and n
R_n^m	Resistance (transformer or transmission line) between nodes m and n

Note. GIC = geomagnetically induced current; LP85 = Lehtinen and Pirjola (1985); T1L = autotransformer T1's common winding.

3.2. Starting With Substation-Level Network Representation and Calculation

We will describe the standard formulation of the LP85 method first because the extended method used in the present paper is based on this formulation. The symbols used for the LP85 method, and the subsequent extension, are listed and described in Table 2. In this section we use the nodal network representation shown in Figure 2a. In the LP85 method each substation is represented as a node (l, m, and n in Figure 2a) and a resistor, R_{trans}. The resistor represents the combined resistance of every transformer within that substation. Each substation is earthed through the EGR, R_e. Nodes are connected by a single transmission line resistor, representing a single phase of the three-phase transmission lines (e.g., $R_{line}^{m,n}$ connecting nodes m and n).

The first step in calculating the GICs in the nodal network representation is common to both the substation-level and transformer-level models. We calculate the current source due to GIC, $J_{m,n}$, along each transmission line by

$$J_{m,n} = \frac{1}{R_{line}} \int_m^n \vec{E} \cdot \vec{ds}. \tag{1}$$

The integration is adding the electric field $\vec{E}$ along the path of the ith transmission line that connects the mth and nth substations, with line elements $\vec{ds}$. The resistance of a single phase of that transmission line is R_{line}. A vector of current sources is built up by performing this operation on every transmission line.

The resistance of the network is described mathematically by two matrices: the network admittance matrix, **Y**, and the earthing impedance matrix, **Z**. In the network admittance matrix, the off-diagonal elements contain the negative admittances ($-Y_{m,n} = -1/R_{line}^{m,n}$) of the lines connecting nodes m and n. The diagonal elements are formed by summing the admittance of every transmission line into each node. Assuming that all substations are far enough away from each other that the GIC flowing to Earth at one node does not affect the voltages at another node, the earthing impedance matrix is diagonal. Each diagonal element of **Z** is the EGR of that node. In the case of the substation-level calculation, each nth element of **Z** is $R_{sub}^n + R_e^n$. GIC varies slowly compared to the 50-Hz AC power so we assume that a DC treatment is sufficient and Y and Z are therefore assumed to be real, following most previous GIC modeling studies. We note that the network inductance can be high so some transient time lag of the GIC could be introduced, which we are not representing.

The vector of substation-level GICs, $\bar{I}_{sub}$, flowing to Earth at each substation is then calculated by

$$\overline{I_{sub}} = (\mathbf{1} + \mathbf{YZ})^{-1} \bar{J} \tag{2}$$

following LP85.

3.3. Transformer-Level Network Representation

We have represented each transformer in a specific substation by adapting the node and connector network representation of LP85, using the techniques described in Boteler and Pirjola (2014). Three nodes of LP85's substation-level node and connector network representation are shown in Figure 2a, where the *n*th substation is represented by the single resistor, R^n_{trans}. However, it is clear from the Single Line Diagram of Invercargill (INV) substation in Figure 2b that real substations are more complicated than this and cannot be represented by a single resistor. The block diagram in Figure 2c shows how we have represented this example substation in the nodal network representation. That representation allows a modification of the nodal matrix calculation method to calculate GIC flowing to Earth at each substation and the GIC flowing through each transformer winding in our modified method.

We show INV as an example of this technique because it is the simplest substation in the network that exhibits all of the key features that we need to represent:

1. multiple voltage levels
2. parallel transformers
3. autotransformers
4. normal transformers

The Single Line Diagram in Figure 2b includes various disconnectors (three-digit numbers), circuit breakers (three-digit numbers in boxes), bus connections, and other features that are of little interest to a GIC modeler. Transmission lines to other substations are indicated by lines continuing out of the top (220 kV) and bottom (110 kV) of the figure. The key features for GIC modeling are the three transformers near the bottom of Figure 2b (labeled T1, T3, and T5). T1 is an autotransformer with the series winding connected to 220 kV, the common winding connected to the 0-V node, and a tap at 110 kV as shown in Figure 2c. T1's function is to convert 220 kV power to 110 kV but from the perspective of GIC the DC resistance of the windings provide a path for GIC to flow between each of the three nodes. T3H and T5H are the high-voltage sides of "normal" transformers, which convert 220 kV to local distribution voltage. Only the high-voltage side is shown because the local distribution lines connecting to the low-voltage side have relatively high resistances and short lengths compared to the high-voltage transmission lines. Therefore, we assume that local distribution lines do not contribute significantly to GIC, and consequently, these circuits are not modeled.

However, a problem arises in trying to fit multiple transformers into the LP85 network representation. This problem occurs when trying to fit multiple nodes within the same substation, representing different voltage buses, to the nodal representation of LP85. It is simple enough to represent each transformer winding as a DC resistance that connects each high-voltage node to the 0-V node. The neutral connection (or earthed connection) of each transformer is connected to the Earth mat then to local Earth through the EGR at the same substation. In this case, the simple representation of $R_{\text{node}} = R_{\text{e}} + R_{\text{trans}}$ with a single node per substation, which is used in LP85's representation, does not work. This is because the EGR is in series with several parallel transformers, each of which is also connected to a high-voltage bus within the substation. Calculation of the GICs flowing to Earth through each of these transformers using the LP85 method would require a calculation of the current through a resistor in series with parallel resistors that the simple network representation is not capable of representing. Hence, calculating the GIC through each transformer requires a small modification of the LP85 approach. We call this modified approach a transformer-level network representation, to calculate transformer-level GICs. In the following subsections we show how we deal with multiple nodes within a single substation and different transformer types.

As an additional complication, Transpower have installed neutral Earth resistors (NERs) in series with transformers at some substations. These NERs were installed to reduce the level of HVDC earth return current that enters the network at locations around the South Island when the HVDC link is operating in earth return mode, as described by Manus Mac et al. (2017). These NERs also have the effect of reducing the GICs flowing to ground by a simple increase in the effective resistance connecting the 0-V node to the higher-voltage nodes within a substation. These NERs are included in the network representation at substations by adding the resistance of the NER to transformer winding resistance where they are installed. The case study for the ISL substation we present later in this study (in section 4.3) includes the NERs installed there.

3.3.1. Multiple Voltage Levels Within a Substation

In our transformer-level approach, each high-voltage bus within a substation is represented as a node as shown for the 110 and 220 kV buses in Figure 2c. These nodes and color-coded buses have also been added to Figure 2b for comparison. Note, the Earth node is not shown in Figure 2b. Each of these high-voltage nodes is connected to local Earth by an infinite "virtual resistor" for consistency with the LP85 method, following Boteler and Pirjola (2014). The resistance of these virtual resistors is represented as 10^{10} Ω to avoid dividing by 0 in the matrix inversion of equation (2), as noted by Boteler and Pirjola (2014) and Divett et al. (2017). In reality, the "leakage current" will flow into local Earth through the noninfinite insulators in the substation but is not large enough to be of interest. In the model it is in the order of 10^{-10} A.

The Earth mat, or 0-V node, is connected to local Earth by the EGR. Transpower provided the most recent measurements available of EGR for each of the 29 earthed substations on the South Island's high-voltage transmission network. The location of all 29 are shown in Figure 1. Across the South Island the EGR values range from 0.04 Ω at SDN to 4 Ω at KUM. These values differ by 2 orders of magnitude due to factors such as underlying rock type, local soil type, and moisture content. The other 35 substations are not earthed on the high-voltage side of the transformer because they use delta-wye transformers, where any Earth connection is on the local distribution side of the transformer. These 35 unearthed substations do not provide a path for GIC to flow into or out of the high-voltage transmission network because there is no direct connection to local Earth at these locations. The EGR at unearthed substations is assumed to be 10^{10} Ω, following Divett et al. (2017).

In the example substation shown in Figure 2 we now have three nodes, each of which is connected to local Earth by either an EGR or virtual resistor, consistent with the LP85 network representation. Using the terminology of LP85, the high-voltage winding of a normal transformers such as T5H or T3H at INV become "line" resistances connecting the 0-V node and 220 kV node in Figure 2c. For the autotransformer T1 with a tap at 110 kV the series winding (T1H) connects the 220 kV node to the 110 kV node and the common winding (T1L) connects the 110 kV node to the 0-V node. High-voltage nodes (both 110 and 220 kV) are also connected to the rest of the network through resistive transmission lines, in most cases multiple lines per node. These transmission lines are represented by the green resistive element in Figure 2c with the current source, *J*, induced in that line by the electromotive force shown in parallel with these transmission lines, in the same way that they are represented in the LP85 method.

3.3.2. Autotransformers, Normal Transformers and Parallel Transformers

The DC resistance of each common, series, high-voltage, or low-voltage winding is found by dividing the phase-neutral DC winding resistance of a single phase by 3. Thus, the DC resistance represents the resistance to a DC flowing through all three of the three-phase windings in parallel. The DC resistance of every high-voltage transformer in the South Island network was supplied by Transpower. Hence, these are the actual resistances to GICs flowing through the network rather than the approximations, as used in many previous modeling studies.

It is common for more than one transformer to connect the same buses in parallel within a substation. These parallel transformers are represented in our model by adding the resistances in parallel when constructing the network admittance matrix in the same way that Divett et al. (2017) did for parallel transmission lines.

Autotransformers such as INVT1, shown in Figure 2, connect two high-voltage nodes as well as Earth. In contrast, each winding of a normal transformer only provides a direct connection between one high-voltage node and Earth. Our example substation shows only the high-voltage side of two normal transformers (INVT3H and INVT5H) connecting 220 kV to 0 V. The low-voltage side of these transformers connects to the local distribution (33 kV) side of the substation and is not modeled in our representation for reasons described earlier in section 3.3.

The significance of these two types of transformer to GIC is that autotransformers provide a more direct path for GIC to couple between two different voltage lines than normal transformers. In the case of a normal transformer connecting the 220 kV network to the 110 kV network, the GIC entering the substation on a 220 kV transmission line must flow through the high-voltage side of the transformer, then through the Earth mat, before flowing through the low-voltage side of the transformer and into the transmission lines on the 110 kV network. This is one example of how the detailed electrical connectivity inside a substation can make a significant difference to the GIC magnitudes in individual transformers.

3.4. Calculating Transformer-Level GIC

Boteler and Pirjola (2014) provide a method to represent a combination of autotransformers and normal transformers in LP85's network representation that does not require off-diagonal elements to the earthing impedance matrix. Significantly, this method correctly represents the transformer resistance between different voltages in the network. This allows the correct calculation of GIC flowing between subsections of the network, which supply different voltages. This impedance between voltages is not represented at all in the simpler network representation and may yield a reduced GIC for lower voltage sections of the network. It may also reduce the impact of the lower voltage subnetworks on the higher voltage sections.

We now have every transformer within every earthed substation in the South Island network represented in a way that is consistent with the LP85 network representation, as shown in Figure 2. We can then use matrix calculations to calculate the GIC through the DC resistance of each transformer winding using the following approach. The transformer winding resistances are used to calculate impedance between nodes within a substation in the network admittance matrix, **Y**. The line resistance of a single phase of each transmission line, measured and provided by Transpower, is used for the resistance of transmission lines connecting substations. The EGRs, R_e^n, which are either the EGR supplied by Transpower or a practically infinite "virtual resistance," are then used to build the earthing impedance matrix, **Z**. This means that by applying equations (1) and (2) we have now calculated the GIC flowing to Earth through every earthing resistor. In the case of the 0-V nodes the calculated GIC is the substation-level GIC, I_{sub}, representing the total GIC flowing to local Earth through the EGR at a given substation. However, in the case of each high-voltage node, including the virtual resistor is essential to calculate the GIC flowing through transformer windings, even though the modeled current in the virtual resistor is on the order of 10^{-10} A.

Within a substation the GIC through each transformer, I_{trans}, is calculated by two simple applications of Ohms law, as described by Boteler and Pirjola (2017). First, we calculate the node voltage, relative to the local substation Earth, by

$$\overline{V_e} = \overline{I_{sub}} \cdot \overline{R_e} \tag{3}$$

as an element-wise multiplication of the vectors of GIC flowing to Earth, I_{sub}^n through the EGR at each of the nodes, R_e, including the virtual resistors.

Then, we calculate the voltage difference between each node from

$$V_n^m = V_e^n - V_e^m \tag{4}$$

for all nodes within every substation. Then, finally, the GIC flowing through the DC resistance of each winding of each transformer, R_{trans}, can be calculated using

$$I_{trans} = \frac{V_n^m}{R_n^m} \tag{5}$$

also calculated element-wise in a vector operation. It should be noted that V_e^n and V_e^m are relative to local Earth for each specific substation. When we use the full matrix method to calculate the voltage difference between nodes, V_n^m, and the current flowing between nodes, I_{trans}, we find both a voltage for nodes at different substations (across transmission lines) and the voltage difference between transformers within a substation. While V_n^m does represent the expected voltage difference at each node within a specific substation, the calculated current flowing between nodes at different substations does not represent the GIC flowing through that transmission line. To be clear about this point, equations (1)–(3) do include the effect of different local Earth voltages, while this effect is removed in equations (4) and (5).

4. Results: Transformer-Level GIC Across the South Island

4.1. Calculated Substation-Level GIC Across the South Island With Transformer-Level Network Representation

GICs calculated using the earlier, substation-level network representation (Divett et al., 2017) for each of the earthed substation in the South Island network are shown in Figure 3a. In contrast, the substation-level GICs calculated using the *transformer-level* network representation are shown in Figure 3b. In both cases we used the electric field calculated by the thin-sheet model with a uniform magnetic field and conductance model derived from magnetotelluric measurements, geology, and bathymetry described in section 3.1.

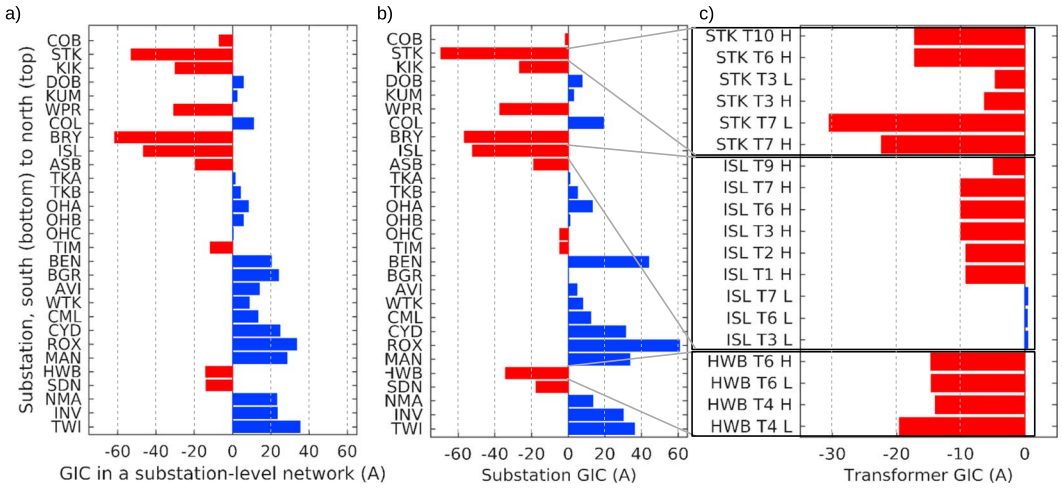

Figure 3. (a) Total substation geomagnetically induced current (GIC) flowing to Earth at each substation using the substation-level network representation from Divett et al. (2017), (b) substation-level GIC using the transformer-level network representation, and (c) the transformer-level GIC flowing through each transformer within three key substations.

In most of the southern part of the network the transformer-level representation results in GICs that are about 25% higher than GICs using the substation-level representation. Doing the modeling at the transformer-level we better include multiple voltage levels so we get more accurate results, relative to the earlier substation-level modeling. The GIC magnitude at some of the central hydro dam (ROX, BEN, and OHA), and Dunedin (HWB) substations are significantly higher with the transformer-level of detail represented. AVI, TIM, BRY, NMA, and BGR are the only locations with smaller GICs in the transformer-level network representation. BGR is an unusual case because it is part of the HVDC link to the North Island. GIC is 0 A at BGR in the transformer-level network because it is not actually connected to the AC network. This is a demonstration of where a transformer-level representation of the network is crucial to understanding GIC risk. If we assumed the substation was a 0.5 Ω resistor (as commonly applied in GIC modeling studies) we would incorrectly calculate the GIC to be 24 A when in fact it should be 0 A. GIC at nodes on Tasman (COB) and the West Coast's (DOB, KUM, and OTI) 66 kV nodes are of similar size in both models. The 25% increase in GIC magnitude for multiple locations demonstrates the importance of including this level of detail to represent each substation. The previous simplified representation not only does not include the level of detail required to compare against observations and identify individual transformers at risk but also underrepresents the modeled GIC compared to a transformer-level network representation.

The highest magnitude of modeled substation-level GIC in the South Island network is $I_{sub} = -68$ A at the Stoke (STK) substation. This is surprising, as it is not a location that is known to have been damaged by GICs. There are also no measurements of GICs at STK, which highlights the value of modeling GIC in this way. We have identified STK as a location that is at risk and suggested that Transpower install monitoring equipment here. The high GIC at STK is probably caused by STK's location at the edge of the electrical network and the local topography. Near STK the coast rises abruptly to mountainous terrain in a sharp corner of Tasman Bay. The resulting steep gradient of ground conductance leads to a strong geoelectric field aligned parallel with transmission lines that run northwest and southeast from STK. The uniform magnetic field we have used in this model also contributes to high GIC at STK. During a real geomagnetic storm the magnetic field variation is likely to be of lower magnitude to the northern end of the South Island compared to the southern end. This would reduce the impact of GIC on STK, relative to what our modeling suggests. However, it also possible that during a large storm the geomagnetic variation would move further north with the expansion of the auroral oval, in which case the calculated GIC might be representative of a large storm.

The next highest magnitude of substation-level GIC is $I_{sub} = 61$ A at ROX, which is also not a location known to experience high levels of GIC. This is easily explained by looking at the transformer level for this substation. There are eight normal transformers connected in parallel at ROX, which are electrically similar as well as one autotransformer. The GIC is divided more or less evenly through each transformer. The resulting transformer-level GIC at ROX is only 16 A through the autotransformer's series winding, 6 A through the

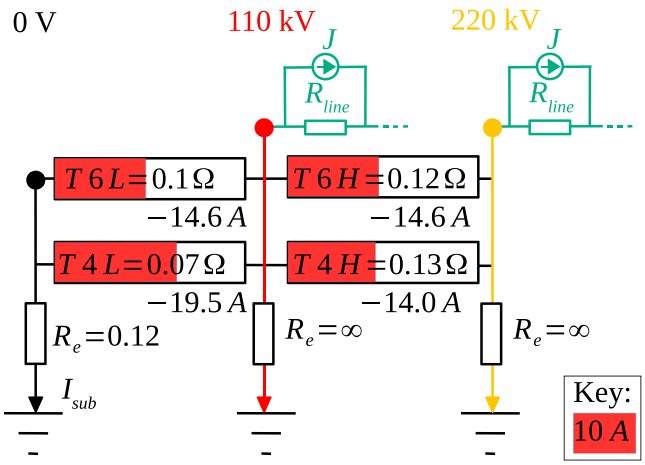

Figure 4. Block diagram showing the DC characteristics of transformer windings at Halfway Bush substation. The modeled GICs through those transformers are represented by the length of the red boxes and is written below each transformer.

common winding, and 11 A flows through each of the eight normal transformers. Hence, although at the substation-level the GIC looks high at ROX, the transformer-level GIC at ROX is only one third to a half of the highest transformer-level GICs that are shown in Figure 3c.

The next highest magnitude substation-level GICs are at the two substations at Christchurch (BRY and ISL) and BEN (Figure 3b). The peak observed GICs through transformers at BRY were approximately one third those at ISLT6 during the 6 November 2001 storm (Manus Mac et al., 2017). The transformer-level modeled GIC at BRY is 19 A, about twice the modeled GIC at ISLT6. Further work is required to understand the difference between the ratio of GIC that occurred at BRY and ISL. The uniform magnetic field used in this model may account for some of this difference between modeled and observed ratios as BRY and ISL. This is possible because ISL and BRY are connected to distinctly different sets of transmission lines despite being located in the same city. Those transmission lines traverse different parts of the country so can potentially pick up induced current from different electric fields particularly due to coastal effects and spatial variation in the magnetic field.

On the other hand we do see a reasonable agreement in the ratios of transformer-level GIC at ISL and HWB. If we only looked at the ratio of modeled substation-level GIC at HWB and ISL we would conclude that $I_{HWB}/I_{ISL} = 0.67$. This substation-level ratio is in stark contrast to the ratio of $I_{HWBT4}/I_{ISLT6} \approx 3$, which comes from observations of transformer-level GIC at several storms over the period of Transpower's GIC observations at both substations (2013 to 2015; Rodger et al., 2017). The very different ratios are easily explained by looking at the transformer-level modeled GICs for the two substations.

This difference in ratio of GIC at HWB and ISL is the most significant result of the comparison between substation-level GIC and transformer-level GIC in Figures 3b and 3c. The difference between the observed ratio and modeled substation-level ratio demonstrates the importance of modeling transformer-level GIC instead of substation-level GIC. The substation-level GIC at ISL is 52 A, among the highest in the South Island. However, the highest modeled transformer-level GIC at ISL is only 10 A, at most, only half that at HWBT4L. Thus, calculating the transformer-level GIC shows that while ISL is still exposed to a GIC risk, HWB is at a significantly higher risk from GIC than ISL. This prediction would not have been possible if the calculation had stopped at the substation level and more accurately represents the observations of GICs and impacts on transformers in the South Island during storms.

4.2. GIC Through Individual Transformers at HWB

In Figure 3c we zoom in to focus on the modeled transformer-level GIC at key substations in the network. We choose to focus on these locations because transformers at HWB and ISL have exhibited high levels of observed GIC (particularly at HWBT4 and ISLT6) in the past and due to the damage at HWBT4 in 2001.

The different transformer characteristics and connections impact GIC depending on how each substation and each transformer within the substation are designed. We show how these designs impact the transformer level GIC for our three test case substations on the block diagrams in Figures 4–6. We label the DC resistance

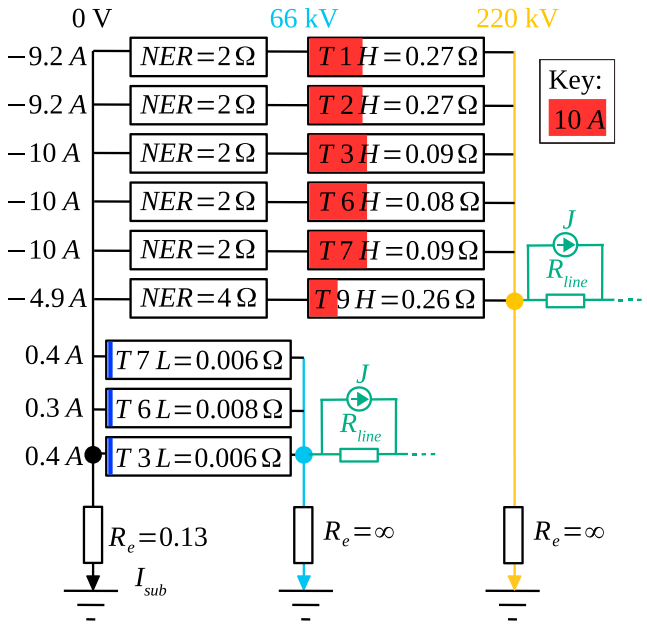

Figure 5. Block diagram showing the direct current characteristics of transformer windings and neutral Earth resistors (NERs) at Islington substation. The modeled GICs through those transformers are represented by the length of the red (negative) and blue (positive) boxes and written on the left.

on the rectangular box that represents the DC resistance of each transformer winding. The magnitude of the transformer-level GIC in each transformer is shown in these figures by the length of the colored bars.

The DC resistance of each transformer winding and substation design contribute to the high levels of GIC at HWB. HWB substation has three voltage nodes: 0 V, 110 kV, and 220 kV, represented in Figure 4 by black, red, and yellow nodes and lines, respectively. The multiple connections of the 110 and 220 kV nodes to the rest of the South Island's transmission network are represented by transmission line resistors, shown in green in Figure 4 for each node. Both HWBT4 and HWBT6 are autotransformers connecting 220 kV and 0 V nodes with a tap at 110 kV. The series and common windings of HWBT4 are HWBT4H and HWBT4L, respectively, and likewise for HWBT6.

The transformer-level modeled GIC at HWB very simply highlights the important differences between the substation-level GIC and transformer-level GIC shown in Figures 3b and 3c. The substation-level GIC at HWB does not look remarkable compared to substations such as ROX. However, it is apparent that the GIC through individual transformer windings is significantly higher. This is due to the low number of transformers at HWB for the GIC to be spread between, the distribution of their resistances, and the specific way that these transformers are connected to voltage buses within HWB substation.

As noted above, in Figure 4 the transformer-level GICs flowing through the series and common windings of each of the two autotransformers at HWB are shown by the length of the red bars inside each box, respectively, in Figure 4. With the GICs and resistances shown in this way it is clear that the high transformer-level GICs (particularly the 19.5 A flowing through HWBT4L) can be explained by a combination of four aspects of the network:

1. low line resistance on the 220 kV lines,
2. higher line resistance on the 110 kV lines,
3. the parallel connection of two autotransformers, and
4. the relative resistance of those autotransformer windings.

Due to these factors, our modeling suggests that HWBT4L will experience higher GIC (and thus higher hazard levels) than other transformer windings in the HWB substation. Further, our modeling indicates that the HWBT4L transformer winding will have the highest GIC in the South Island, with the possible exception of STK, as discussed in section 4.4.

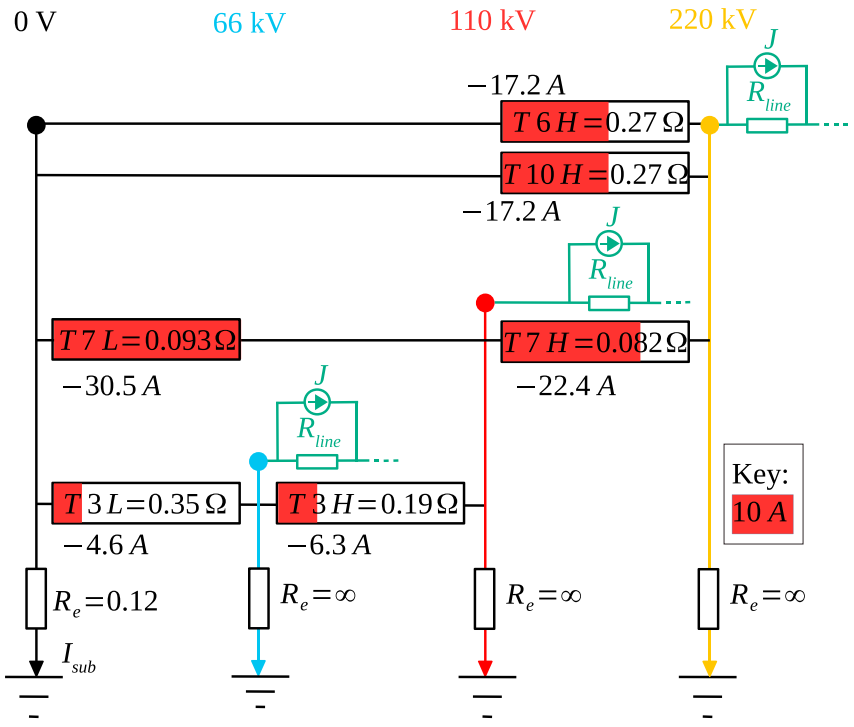

Figure 6. Block diagram showing the DC characteristics of transformer windings at Stoke substation. The modeled GIC through those transformers is represented by the length of the red boxes and written below (above for T6H) the transformer.

4.3. GIC Through Individual Transformers at ISL

The block diagram of the resistances and connections for transformer windings at the ISL substation are shown in Figure 5. Again the GIC for each winding is indicated by the length of red (negative current) or blue (positive current) bars. Note, the blue bars are very short due to the low level of GIC in those transformers. This diagram helps explain the flow of GIC at ISL in the same way that the block diagram helps explain the differences in current through each transformer winding at HWB. However, the transformers at ISL are all normal transformers with ISLT3, ISLT6, and ISLT7 designed to convert power from 220 to 66 kV. ISLT1 and ISLT2 are designed to convert power from 220 kV to the local distribution voltage of 33 kV. The low-voltage side windings on the local distribution network are not represented in our representation or shown in Figure 5 due to the high resistance of the connection to Earth of the local 33 kV network. ISLT9 has a 12.5 kV low-voltage winding and is a dedicated transformer for the Static VAR Compensator, to provide regulation and stability to the power system.

The other major difference between ISL and HWB is the NERs in series with some transformers. The NERs' function is to suppress the HVDC earth return currents that enter the network at ISL when the HVDC link is operating in earth return mode (Manus Mac et al., 2017). The NERs also act to suppress the quasi-DC GICs from flowing through the high-voltage side windings at ISL. The high resistance of the NERs, relative to the resistance of the high-voltage side transformer windings reduces the GIC that will flow to ground through this path. In fact, adding NERs is a technique sometimes used to mitigate the impact of GICs on electrical networks (for example, Hussein, 2016). The NERs serve a dual purpose here as they act to even out the level of GIC that flows through each of ISLT1H to ISLT7H.

The modeled GIC through each of these transformer windings only varies between 9.2 and 10 A. This is despite the resistance of these transformer windings varying by a factor of 3.4. This consistent level of GIC is due to the similarity of the combined total resistance of NER plus R_{trans} for each of these transformer windings. Of these similar levels of GIC, the GIC through ISLT6H is slightly higher, due to its slightly lower resistance. Further, the significantly lower modeled GIC flowing through ISLT9H is due to the resistance of the NER in series with ISLT9H being double that of the other NERs at ISL. This high NER is installed to protect the Static VAR Compensator during a GIC event.

At ISL, the modeled GIC through T3H and T7H is the same, in good agreement with the observations in Table 1. Further, the modeled GIC through T3H is twice that through T9H, also in fairly good agreement with the factor 3 seen in the observed GICs in Table 1. However, the modeled GIC through T6H is very similar to that through T3H, which does not match the observed factor of 3 between the two transformers. It is not clear why the observed GIC at T6H is 3 times that through T3H, given that the resistance of these transformers is similar. The resistance of the NERs and transformer windings are nearly identical. We are currently working with Transpower to understand why that difference occurs.

An interesting feature of the modeled GICs at ISL is the difference in direction of the GICs flowing through the three low-voltage-side transformer windings (ISLT3L, ISLT6L, and ISLT7L), shown by the blue bars in Figure 5 (again, note, the blue bars are very small because the GIC is much lower than other GIC shown). This indicates that while GICs flow out of the Earth mat and into the 220 kV transmission lines through ISL's high side windings, GIC flowing through the low side windings flows into the Earth mat and out of the 66 kV transmission lines. The magnitude is small, mostly due to the high line resistance of the 66 kV network that connects the low-voltage side transformer windings to the rest of the network. This change in direction of the GIC demonstrates the complex path that GIC can take through high- and low-voltage side windings of transformers at the same substation.

To first order the direction of the GIC does not change the impact on a transformer. However, if GIC flows in the same direction through both windings of a common-core transformer (such as an autotransformer), then the magnetic flux adds constructively. On the other hand if the GIC flows in opposite directions in each winding (as is the case for T3, T6, and T7) then the magnetic flux can cancel to some degree, reducing the impact of the GIC on the transformer. However, the magnetic flux of the low side of these transformers at ISL is very low due to the low magnitude of the GIC and the relatively low number of turns on the 66 kV windings compared to the 220 kV windings. Despite having little impact on the GIC hazard, this effect is a significant difference between the route that GIC flows through the autotransformers at HWB and the normal transformers at ISL. Note also that the direction of GIC flowing from the high-voltage bus to the Earth mat is conditional on the direction of the magnetic field vectors chosen for this modeling study. In reality, the electric field is an elliptically rotating vector in the horizontal plane, under the plane wave assumption. Hence, the direction of the GIC will swap direction every half period as the direction of the electric field rotates by 180°, as shown for substation-level GIC by Divett et al. (2017).

4.4. GIC Through Individual Transformers at STK

We also present detailed results for STK substation where there are currently no GIC observations. STK shows the highest level of modeled transformer-level and substation-level GICs in the network. STK is also an interesting substation in that it has a bus for each of the three voltage levels of the AC transmission network (50–66, 110, and 220 kV).The transformer-level GICs at STK are of greater magnitude and has greater differences within the substation than that at either HWB or ISL, as shown in the block diagram in Figure 6. STK has a bus for each of the three primary voltages used in the South Island network (66, 110, and 220 kV). These are connected by a combination of autotransformers (STKT3 and STKT7) and normal transformers' high-voltage side windings (STKT6H and STKT10H).

As seen in Figure 6, the highest GIC at STK flows through the T7 autotransformer, connecting the 220 kV bus to Earth, with a tap at 110 kV. The reason for this is largely due to the difference of the resistance of each possible path connecting the 220 kV bus to the 0 V node in Figure 6. The DC resistance of the T7 autotransformer is $R_{STKT7L} + R_{STKT7H} = 0.175\Omega$ compared to the relatively higher resistance (0.27 Ω) of either of the normal transformers. Interestingly, the GIC flowing through the common winding of STKT7 is higher than that flowing through STKT7's series winding. This higher GIC flowing through the higher-resistance windings of the same autotransformer is due to the current through STKT7L being split between T7H and the 110 kV transmission lines. The current through STKT7L is negative so 8.1 A of the GIC that flows from Earth, through STKT7L, subsequently flows into the 110 kV transmission lines, while the remaining 22.4 A flows on through the series winding of STKT7 and into the 220 kV transmission network.

The GIC flowing through STKT3 is significantly lower than that flowing through other transformer windings at STK. This is due to the relatively higher resistance of these windings, compared to other transformers at STK, and the relatively higher resistance of the 66 kV transmission lines compared to the 220 kV transmission lines. The GIC through STKT3H is higher than that through the low-voltage common winding. The difference between the two currents ($I_{T3H} - I_{T3L}$) flows into STKT3H from the 66 kV transmission lines.

5. Discussion

Comparisons of the modeled GICs in this study with observations of GICs made by Transpower (Rodger et al., 2017) show a reasonable agreement with the reported typical relationship between GIC magnitude at HWBT4L and ISLT6H. Rodger et al. (2017) compared the observed GICs at ISLT6 and HWBT4 during five large space weather events occurring between 17 March 2013 and 22 June 2015. In these events the peak GIC flowing through HWBT4 was ˜3 times that flowing through ISLT6H. By comparison, the ratio of modeled GIC through ISLT6H and HWBT4L is 2. While the modeled and observed ratio are not in full agreement, they are certainly comparable given the inherent simplifications made and are a great improvement over the earlier substation-level results.

It is possible that some of the difference between measured and modeled GIC ratios at different transformers is due to the modeling assumption that the magnetic field is spatially uniform in a single orientation. If the magnetic field variations were stronger in the south of the South Island during a geomagnetic storm, and varied in time with the changing orientation of the geomagnetic disturbance, it could account for the increased observed GIC at HWB compared to ISL that is not seen in the modeled GIC. Further work to represent a more realistic spatial and temporal variation of the magnetic field, for example, during the St. Patrick's Day 2015 storm is ongoing.

However, the modeled transformer-level GIC does a far better job of capturing the observed ratio of GICs at ISLT6H to HWBT4L than the substation-level GIC does. The highest modeled transformer-level GIC at a site where Transpower measure GIC is at HWBT4L, matching observations of the 2 October 2013 event. Manus Mac et al. (2017) showed that the peak GIC observed at HWBT4 was 48.9 A, compared to the next highest observed GIC of 19.1 at ISLT6. On the other hand, the modeled substation-level GIC at HWB is actually smaller than that at ISL, where HWB GIC is 0.67 of the GIC at ISL. Further, using the common assumption that each substation can be represented by a single resistance of 0.5 Ω, this ratio (0.33) was even further from the observations. Hence, the transformer-level GICs calculated in the present study leads to a large improvement in capturing the difference between GIC at different locations on the network when compared to models where the substation is assumed to be a single resistance to Earth. Ratios of observed GICs through transformers within ISL during five recent storms show that some of the modeled ratios of GIC are close to observations while the ratio of GIC through ISLT3H to ISLT6H does not match observations well. We are working with Transpower to understand this difference. It is not clear why the GIC through ISLT6H is so much higher than ISLT3H and ISLT7H based on the reported resistances for these transformers.

Significantly, our method correctly represents the transformer resistance between subsections of the transmission network that are at different voltages. The transformer-level network representation provides a more complete representation of the resistance to current between these subsections of the network compared to a network where each substation is assumed to be a single resistance to Earth. In the INV example substation in Figure 2 the resistance of the autotransformer T1H connects the 220 kV and 110 kV nodes, providing extra resistance to GIC flowing from 220 kV transmission lines to the 110 kV transmission lines or vice versa. Normal transformers such as T3 at ISL impede current flow between subsections even further, as they have two windings separating the buses at different voltages. This resistance between voltages is not represented in previous substation-level network representations. Hence, the substation-level network representation would be expected to calculate higher GICs for the low-voltage sections of the network, compared to the transformer-level calculations in the present paper. However, it is worth noting that it is uncommon for *Space Weather* researchers to have access to the level of detail that we have for the New Zealand network (Hapgood & Knipp, 2016), as such other regions may not be able to develop such a detailed representation.

6. Conclusions

We have modeled transformer-level GICs in the South Island of New Zealand's high-voltage transmission network. The geoelectric field for the New Zealand region was calculated using the thin-sheet method of Vasseur and Weidelt (1977) by Divett et al. (2017). The geomagnetic field variation was assumed to be spatially uniform across the whole domain, with a magnitude of 500 nT in the direction 50° east of north at a period of 10 min. This single period provides a peak $dB/dt = 50$ nT/min. We chose this magnitude and period to be representative of a moderately large storm without attempting to capture the spatial and temporal variability of any particular geomagnetic storm event. This is an intentional idealization in order to clarify and simplify the presentation of the transformer-level network representation and calculations.

The modeled electric field was applied to the modified LP85 model. We modified the network representation developed by LP85 to account for a single phase of every transformer in the network to give a transformer-level network representation of the South Island transmission network. This more detailed representation is based on the methods for representing autotransformers and normal transformers in Boteler and Pirjola (2014). DC resistances for transformers, a single phase of the three-phase transmission lines and EGR were supplied by Transpower. We calculated the GIC through each transformer winding using Boteler and Pirjola's (2017) extension of LP85's method.

The modeling indicates that the transformer-level GIC is highest at the STK substation, which is not a location where GICs are being monitored at this time. As a result of this study we have recommended future monitoring of GIC at STK. Apart from STK, HWBT4 had the highest modeled GIC, matching observations of GIC during the 2 Oct 2013 event. The ratio of modeled GIC at HWBT4 to ISLT6 is 2. This is close to the ratio of 3 found by Rodger et al. (2017) for 2 years of observations at the two substations. It is certainly an improvement compared to the factor of 0.67 if we compare results at the substation-level only. This shows the importance of calculating transformer-level GIC.

The modeled GIC flowing through each transformer winding within a substation can be quite different even at the same substation. In fact, due to network configuration and transformer connections within a substation, the current through series and common windings of a single autotransformer can be quite different. Using the block diagrams of Figures 4 to 6, we can explain how the differences in transformer-level GICs occur due to the combination of resistances and connections of transformers within a substation. This supports and helps explain the observational findings of Manus Mac et al. (2017) and Rodger et al. (2017). We believe that this is the first time that modeled transformer-level GICs, calculated using an electric field that included the variations due to ground conductance, have been compared to an extensive set of GIC measurements.

At both STK and HWB the highest GICs flow through the series winding of an autotransformer where there are multiple transformers connecting more than one set of transmission lines with different voltages. Not surprisingly, in each case it is the path to ground with the lowest total resistance that is susceptible to the highest GIC. In contrast, at ISL the transformer-level GIC is lower because it is distributed across several parallel normal transformers that are earthed through neutral earth resistors. Autotransformers provide a more direct path for GIC to flow between transmission lines at different voltages, compared to normal transformers where the GIC flows through both windings and the Earth bus. Thus, the transformers that are most susceptible to GIC in a network are those with a combination of three factors: connections to transmission lines that traverse regions of high electric field, transformer configuration, and low transformer resistance.

Acknowledgments
The authors would like to thank Transpower New Zealand for supporting this study. This research was supported by the New Zealand Ministry of Business, Innovation and Employment Hazards and Infrastructure Research Fund contract UOOX1502. Gemma Richardson, Ciaran Beggan, and Alan Thomson were partly supported under NERC grant NE/P017231/1: Space Weather Impacts on Ground-based Systems (SWIGS). The South Island electrical transmission network's DC characteristics and DC measurements were provided to us by Transpower New Zealand with caveats and restrictions. This includes requirements of permission before all publications and presentations. In addition, we are unable to provide the full New Zealand network characteristics directly. Requests for access to these characteristics need to be made to Transpower New Zealand. At this time the contact point is Michael Dalzell (Michael.Dalzell@transpower.co.nz). We are very grateful for the substantial data access they have provided, noting this can be a challenge in the *Space Weather* field (Hapgood & Knipp, 2016).

References

Bailey, R. L., Halbedl, T. S., Schattauer, I., Römer, A., Achleitner, G., Beggan, C. D., et al. (2017). Modelling geomagnetically induced currents in mid-latitude central Europe using a thin-sheet approach. *Annales Geophysicae*, *5*, 751–761. https://doi.org/10.5194/angeo-35-751-2017

Beggan, C. D., Beamish, D., Richards, A., Kelly, G. S., & Thomson, A. W. (2013). Prediction of extreme geomagnetically induced currents in the UK high-voltage network. *Space Weather*, *11*, 407–419. https://doi.org/10.1002/swe.20065

Beland, J., & Small, K. (2004). Space weather effects on power transmission systems: The cases of hydro-Québec and transpower New Zealand Ltd. In *Effects of Space Weather on Technology Infrastructure* (pp. 287–299). Dordrecht: Kluwer Academic Publishers.

Blake, S. P., Gallagher, P. T., McCauley, J., Jones, A. G., Hogg, C., Campanyà, J., et al. (2016). Geomagnetically induced currents in the Irish power network during geomagnetic storms. *Space Weather*, *14*, 1–19. https://doi.org/10.1002/2016SW001534

Boteler, D. (2014). Methodology for simulation of geomagnetically induced currents in power systems. *Journal of Space Weather and Space Climate*, *4*(A21), A21. https://doi.org/10.1051/swsc/2014018

Boteler, D. H., & Pirjola, R. J. (2014). Comparison of methods for modelling geomagnetically induced currents. *Annales Geophysicae*, *32*(9), 1177–1187. https://doi.org/10.5194/angeo-32-1177-2014

Boteler, D. H., & Pirjola, R. J. (2017). Modeling geomagnetically induced currents. *Space Weather*, *15*, 258–276. https://doi.org/10.1002/2016SW001499

Butala, M. D., Kazerooni, M., Makela, J. J., Kamalabadi, F., Gannon, J. L., Zhu, H., & Overbye, T. J. (2017). Modeling geomagnetically induced currents from magnetometer measurements: Spatial scale assessed with reference measurements. *Space Weather*, *15*, 1357–1372. https://doi.org/10.1002/2017SW001602

Chamalaun, F., & McKnight, D. (1993). A New Zealand wide magnetometer array study. *Journal of Geomagnetism and Geoelectricity*, *45*, 741–759.

Divett, T., Ingham, M., Beggan, C. D., Richardson, G. S., Rodger, C. J., Thomson, A. W. P., & Dalzell, M. (2017). Modeling geoelectric fields and geomagnetically induced currents around New Zealand to explore GIC in the South Island's electrical transmission network. *Space Weather*, *15*, 1396–1412. https://doi.org/10.1002/2017SW001697

Erinmez, I. A., Kappenman, J. G., & Radasky, W. A. (2002). Management of the geomagnetically induced current risks on the national grid company's electric power transmission system. *Journal of Atmospheric and Solar-Terrestrial Physics*, *64*(5–6), 743–756. https://doi.org/10.1016/S1364-6826(02)00036-6

Guile, A., & Paterson, W. (1977). *Electrical power systems* (Vol. 2, 2nd ed.). Oxford: Pergamon Press.

Hapgood, M., & Knipp, D. J. (2016). Data citation and availability: Striking a balance between the ideal and the practical. *Space Weather*, *14*, 919–920. https://doi.org/10.1002/2016SW001553

Horton, R., Boteler, D., Overbye, T. J., Pirjola, R., & Dugan, R. C. (2012). A test case for the calculation of geomagnetically induced currents. *IEEE Transactions on Power Delivery*, *27*(4), 2368–2373. https://doi.org/10.1109/TPWRD.2012.2206407

Hussein, A. A. (2016). Novel solutions to suppress adverse effects of geomagnetically induced current (GIC) on power systems (PhD), The University of Memphis.

Koen, J., & Gaunt, T. (2003). Geomagnetically induced currents in the Southern African electricity transmission network. In *2003 IEEE Bologna Power Tech Conference Proceedings* (Vol. 1, pp. 408–414). IEEE. https://doi.org/10.1109/PTC.2003.1304165

Lehtinen, M., & Pirjola, R. (1985). Currents produced in earthed conductor networks by geomagnetically-induced electric fields. *Annales Geophysicae*, *3*(4), 479–484.

Liu, C.-M., Liu, L.-G., Pirjola, R., & Wang, Z.-Z. (2009). Calculation of geomagnetically induced currents in mid- to low-latitude power grids based on the plane wave method: A preliminary case study. *Space Weather*, *7*, S04005. https://doi.org/10.1029/2008SW000439

Manus Mac, D. H., Rodger, C. J., Dalzell, M., Thomson, A. W. P., Clilverd, M. A., Petersen, T., et al. (2017). Long term geomagnetically induced current observations from New Zealand: Earth return corrections and comparison with geomagnetic field driver. *Space Weather*, *15*, 1020–1038. https://doi.org/10.1002/2017SW001635

Marshall, R. A., Dalzell, M., Waters, C. L., Goldthorpe, P., & Smith, E. A. (2012). Geomagnetically induced currents in the New Zealand power network. *Space Weather*, *10*, S08003. https://doi.org/10.1029/2012SW000806

Marshall, R. A., Gorniak, H., Van Der Walt, T., Waters, C. L., Sciffer, M. D., Miller, M., et al. (2013). Observations of geomagnetically induced currents in the Australian power network. *Space Weather*, *11*, 6–16. https://doi.org/10.1029/2012SW000849

Mckay, A. J. (2003). PhD thesis: Geoelectric fields an geomagnetically induced currents in the United Kingdom (PhD thesis), University of Edinburgh.

Mckay, A. J., & Whaler, K. A. (2006). The electric field in northern England and southern Scotland: Implications for geomagnetically induced currents. *Geophysical Journal International*, *167*(2), 613–625. https://doi.org/10.1111/j.1365-246X.2006.03128.x

Overbye, T. J., Hutchins, T. R., Shetye, K., Weber, J., & Dahman, S. (2012). Integration of geomagnetic disturbance modeling into the power flow: A methodology for large-scale system studies. In *2012 North American Power Symposium (NAPS)* (pp. 1–7). IEEE. https://doi.org/10.1109/NAPS.2012.6336365

Parkinson, W. D., & Jones, F. W. (1979). The geomagnetic coast effect. *Review of Geophysics*, *17*(8), 1999–2015. https://doi.org/10.1029/RG017i008p01999

Richardson, G., & Beggan, C. (2017). Validation of geomagnetically induced current modelling code Internal Report IR/17/009 (Tech. Rep.): British Geological Survey. http://nora.nerc.ac.uk/id/eprint/519956

Rodger, C. J., Mac Manus, D. H., Dalzell, M., Thomson, A. W. P., Clarke, E., Petersen, T., et al. (2017). Long-term geomagnetically induced current observations from New Zealand: Peak current estimates for extreme geomagnetic storms. *Space Weather*, *15*, 1–14. https://doi.org/10.1002/2017SW001691

Shetye, K. S., & Overbye, T. J. (2015). Parametric steady-state voltage stability assessment of power systems using benchmark scenarios of geomagnetic disturbances. In *2015 IEEE Power and Energy Conference at Illinois (PECI)* (pp. 1–7). Champaign, IL: IEEE. https://doi.org/10.1109/PECI.2015.7064886

Torta, J. M., Serrano, L., Regué, J. R., Sánchez, A. M., & Roldán, E. (2012). Geomagnetically induced currents in a power grid of northeastern Spain. *Space Weather*, *10*, S06002. https://doi.org/10.1029/2012SW000793

Trivedi, N. B., Vitorello, Í., Kabata, W., Dutra, S. L. G., Padilha, A. L., Bologna, M. S., et al. (2007). Geomagnetically induced currents in an electric power transmission system at low latitudes in Brazil: A case study. *Space Weather*, *5*, S04004. https://doi.org/10.1029/2006SW000282

Vasseur, G., & Weidelt, P. (1977). Bimodal electromagnetic induction in non-uniform thin sheets with an application to the northern Pyrenean induction anomaly. *Geophysical Journal International*, *51*(3), 669–690. https://doi.org/10.1111/j.1365-246X.1977.tb04213.x